Supporting Information

Modulating the Relaxation Dynamics of Na_2Mn_3 Spin-Frustrated Magnets via an Auxiliary Anion Change†

Yongfei Li,[‡a] Xiao Sun,[‡a] Peiqiong Chen,[a] Hou-Ting Liu,[a] Jing Li,*[b] Dan Liu,*[c] Dacheng Li,[a] Jianmin Dou[a] and Haiquan Tian*[a]

[a] Shandong Provincial Key Laboratory of Chemical Energy Storage and Novel Cell Technology, School of Chemistry and Chemical Engineering, Liaocheng University, Liaocheng 252059, P. R. China. E-mail: tianhaiquan@lcu.edu.cn

[b] State Key Laboratory of Physical Chemistry of Solid Surfaces, College of Chemistry and Chemical Engineering, Xiamen University, Xiamen 361005 P. R. China. E-mail: jingli0107@xmu.edu.cn

[c] Institute of Flexible Electronics, Northwestern Polytechnical University, 127 West Youyi Road, Xi'an, 710072, Shaanxi, China. E-mail: iamdliu@nwpu.edu.cn

[‡] These authors contributed equally to this work.

Table S1. Selected bond lengths (Å) and angles (º) for **1**.

Complex 1					
Mn1–O4	1.938(7)	Mn1–O5	1.879(7)	Mn1–O12	2.109(7)
Mn1–O13	1.905(7)	Mn1–N8	1.956(9)	Mn1–N13	2.383(9)
Mn2–O1	1.922(7)	Mn2–O2	1.892(7)	Mn2–O10	2.427(8)
Mn2–O13	1.881(6)	Mn2–N4	1.956(9)	Mn3–O7	1.913(7)
Mn3–O8	1.888(7)	Mn3–O10	2.356(8)	Mn3–O13	1.866(7)
Mn3–N12	1.922(9)	Mn3–N13	2.252(9)	Na1–O1	2.423(7)
Na1–O4	2.336(8)	Na1–O7	2.384(7)	Na1–N1	2.537(11)
Na1–N5	2.584(10)	Na1–N9	2.610(11)	Na2–O2	2.399(7)
Na2–O3	2.496(8)	Na2–O5	2.361(8)	Na2–O6	2.507(10)
Na2–O8	2.412(9)	Na2–O9	2.461(9)	Mn1–O13–Mn2	128.1(4)
Mn1–O13–Mn3	113.9(3)	Mn2–O10–Mn3	83.3(3)	Mn2–O13–Mn3	116.2(4)
Mn1–O4–Na1	124.2(3)	Mn1–O5–Na2	110.2(3)	Mn2–O1–Na1	125.2(3)
Mn2–O2–Na2	107.6(3)	Mn3–O7–Na1	125.2(4)	Mn3–O8–Na2	107.7(3)
Mn1–N13–Mn3	85.9(3)	Mn1···Mn2	3.404(4)	Mn1···Mn3	3.160(6)
Mn2···Mn3	3.180(5)	Na1···Mn1	3.781(4)	Na1···Mn2	3.864(2)
Na1···Mn3	3.820(1)	Na2···Mn1	3.488(8)	Na2···Mn2	3.474(5)
Na2···Mn3	3.486(1)	Na1···Na2	6.260(6)	Mn1–Mn2–Mn3	57.2(4)
Mn1–Mn3–Mn2	64.9(4)	Mn2–Mn1–Mn3	57.8(1)	Na1–O10–Na2	178.1(2)

Table S2. Selected bond lengths (Å) and angles (º) for **2**.

Complex 2					
Mn1–O7	1.906(10)	Mn1–O8	1.862(10)	Mn1–O10	1.894(8)
Mn1–O11	2.105(10)	Mn1–N12	1.953(10)	Mn1–N16	2.368(12)
Mn2–O1	1.904(11)	Mn2–O2	1.874(10)	Mn2–O10	1.897(9)
Mn2–N4	1.972(13)	Mn2–N13	2.261(12)	Mn2–N16	2.335(12)
Mn2–N17	2.878(14)	Mn3–O4	1.908(10)	Mn3–O5	1.868(11)
Mn3–O10	1.892(8)	Mn3–O12	2.093(10)	Mn3–N8	2.018(12)
Mn3–N13	2.404(13)	Na1–O1	2.365(11)	Na1–O4	2.392(11)
Na1–O7	2.422(11)	Na1–N1	2.498(17)	Na1–N5	2.565(17)
Na1–N9	2.570(13)	Na2–O2	2.371(12)	Na2–O3	2.487(12)
Na2–O5	2.365(12)	Na2–O6	2.572(14)	Na2–O8	2.404(10)
Na2–O9	2.448(12)	Na2–O10	2.731(11)	Mn1–O7–Na1	126.3(4)
Mn1–O8–Na2	107.5(8)	Mn2–O1–Na1	125.2(5)	Mn2–O2–Na2	108.6(5)
Mn3–O4–Na1	124.4(5)	Mn3–O5–Na2	110.8(5)	Mn1–O10–Mn2	115.1(4)
Mn1–O10–Mn3	129.8(4)	Mn1–O10–Na2	95.0(4)	Mn2–O10–Mn3	112.3(4)
Mn2–O10–Na2	95.0(3)	Mn3–O10–Na2	96.6(4)	Mn2–N13–Mn3	84.8(4)
Mn1–N16–Mn2	85.7(4)	Mn1···Mn2	3.191(5)	Mn1···Mn3	3.425(3)
Mn2···Mn3	3.146(3)	Na1···Mn1	3.864(9)	Na1···Mn2	3.796(3)
Na1···Mn3	3.811(4)	Na2···Mn1	3.438(7)	Na2···Mn2	3.444(1)
Na2···Mn3	3.487(1)	Na1···Na2	6.229(3)	Mn1–Mn2–Mn3	65.4(2)
Mn1–Mn3–Mn2	57.9(2)	Mn2–Mn1–Mn3	56.6(5)	Na1–O10–Na2	178.3(4)

Table S3. Mn^{II} geometry analysis of **1** and **2** by SHAPE 2.1 software.

	Complex 1			**Complex 2**		
Geometry (CN = 6)	**Mn1**	**Mn2**	**Mn3**	**Mn1**	**Mn2**	**Mn3**
HP-6	29.515	30.781	33.167	31.191	32.096	29.724
PPY-6	26.648	27.407	24.999	26.956	24.136	26.702
OC-6	1.259	1.188	1.951	1.230	1.964	1.143
TPR-6	14.656	15.361	13.992	14.447	13.758	14.686
JPPY-6	29.511	30.337	28.184	29.949	27.062	29.787
Lable	**Shape**	**Lable**	**Shape**	**Lable**	**Shape**	
HP-6	Hexagon (D_{6h})	PPY-6	Pentagonal pyramid (C_{5V})	OC-6	Octahedron (O_h)	
Lable	**Shape**					
TPR-6	Trigonal prism (D_{3h})					

Table S4. The selected energy level of complexes **1** and **2** without magnetic field.

	Complex 1	**Complex 2**
1	0	0
2	7.5745E-14	3.78725E-14
3	16.2956	20.0849
4	16.2956	20.0849
5	20.7587	23.2902
6	20.7587	23.2902
7	22.728	23.8182
8	25.3224	23.8182
9	25.3224	29.2401
10	27.7375	31.336
11	27.7375	31.336
12	29.3502	31.6554
13	55.6594	59.3931
14	55.6594	59.3931
15	63.0455	62.7733
16	63.0455	62.7733
17	63.4825	68.8312
18	63.4825	68.8312
19	64.8999	75.7223
20	64.8999	75.7223

Table S5. Relaxation fitting parameters from least-squares fitting of $\chi(\omega)$ data under zero *dc* field for **1**.

		FR			SR		
T	$\chi_{s,\,tot}$	$\Delta\chi_1$	α_1	$\ln(\tau_1 / s)$	$\Delta\chi_2$	α_2	$\ln(\tau_2 / s)$
1.8	-3.42	16.87	0.287	-1.92	13.20	0.762	-10.71
2.0	-5.75	20.12	0.341	-2.62	5.35	0.547	-11.01
2.3	-8.13	24.74	0.386	-3.30	2.71	0.302	-11.41
2.6	-10.87	28.51	0.385	-3.57	2.22	0.208	-11.70
2.9	-12.01	30.47	0.356	-3.80	3.24	0.362	-11.85
3.2	-15.14	29.14	0.343	-4.07	3.79	0.403	-11.92
3.5	-17.08	29.07	0.321	-4.13	4.47	0.438	-12.16
4	-20.88	30.97	0.274	-4.19	5.62	0.504	-12.33
4.3	-23.29	30.66	0.284	-4.35	5.74	0.490	-12.51
4.6	-25.31	30.43	0.295	-4.52	6.00	0.464	-12.71
4.9	-26.96	31.80	0.255	-4.76	8.46	0.565	-12.93
5.5	-27.71	30.29	0.264	-4.99	8.56	0.583	-13.11
6.0	-28.25	31.43	0.251	-5.16	6.60	0.533	-13.34
6.5	-29.80	33.45	0.199	-5.43	6.96	0.619	-13.58
7.0	-30.11	32.79	0.224	-5.54	3.70	0.507	-13.71
7.5	-30.38	35.57	0.144	-5.64	5.45	0.697	-13.98
8.0	-30.76	34.35	0.170	-5.76	4.99	0.813	-14.13
8.5	-31.02	34.52	0.155	-5.94	4.60	0.816	-14.30

Table S6. Relaxation fitting parameters from least-squares fitting of $\chi(\omega)$ data under zero *dc* field for **2**.

		FR			SR		
T	$\chi_{s,\,tot}$	$\Delta\chi_1$	α_1	$\ln(\tau_1 / s)$	$\Delta\chi_2$	α_2	$\ln(\tau_2 / s)$
1.8	8.88	11.67	0.077	-6.19	-4.20	0.336	6.56
2.0	7.59	11.45	0.070	-6.20	-3.97	0.340	-6.60
2.3	6.31	10.81	0.090	-6.23	-4.05	0.335	-6.67
2.6	5.45	10.18	0.133	-6.31	-4.12	0.350	-6.81
2.9	4.96	9.50	0.178	-6.35	-4.13	0.367	-7.07
3.2	4.23	8.99	0.241	-6.41	-4.15	0.405	-7.31
3.5	3.96	8.28	0.255	-6.50	-4.15	0.401	-7.46
4	3.50	7.57	0.220	-6.69	-4.45	0.336	-7.71
4.3	3.38	7.48	0.301	-6.80	-4.37	0.408	-7.86
4.6	3.04	7.36	0.365	-6.93	-4.42	0.470	-8.23
4.9	2.81	7.89	0.419	-7.17	4.18	0.524	-8.67
5.5	2.54	8.56	0.457	-7.41	-3.99	0.576	-9.07
6.0	2.09	8.24	0.464	-7.62	-3.99	0.594	-9.45
6.5	1.93	8.44	0.441	-7.86	-3.98	0.551	-9.82
7.0	1.72	8.80	0.458	-7.99	-3.92	0.569	-10.05
7.5	1.56	9.91	0.462	-8.19	-3.87	0.569	-10.31
8.0	1.40	11.22	0.450	-8.42	-3.96	0.540	-10.66
8.5	1.35	10.33	0.473	-8.63	-3.90	0.582	-10.79
9.0	1.26	10.73	0.456	-8.81	-3.90	0.530	-10.95
10.0	1.18	11.56	0.449	-9.14	-3.95	0.543	-11.12
11.0	1.03	11.51	0.459	-9.34	-3.94	0.593	-11.35
12.0	0.09	12.04	0.437	-9.60	-3.93	0.524	-11.57
13.0	0.07	11.91	0.443	-9.95	-3.92	0.534	-11.67
14.0	0.03	12.02	0.448	-10.12	-3.91	0.526	-11.80
15.0	-0.06	12.23	0.430	-10.33	-3.87	0.470	-11.92
16.0	-0.11	12.41	0.426	-10.53	-3.82	0.441	-12.04
17.0	-0.18	12.33	0.436	-10.75	-3.85	0.495	-12.10
18.0	-0.21	12.49	0.425	-10.97	-3.89	0.507	-12.16

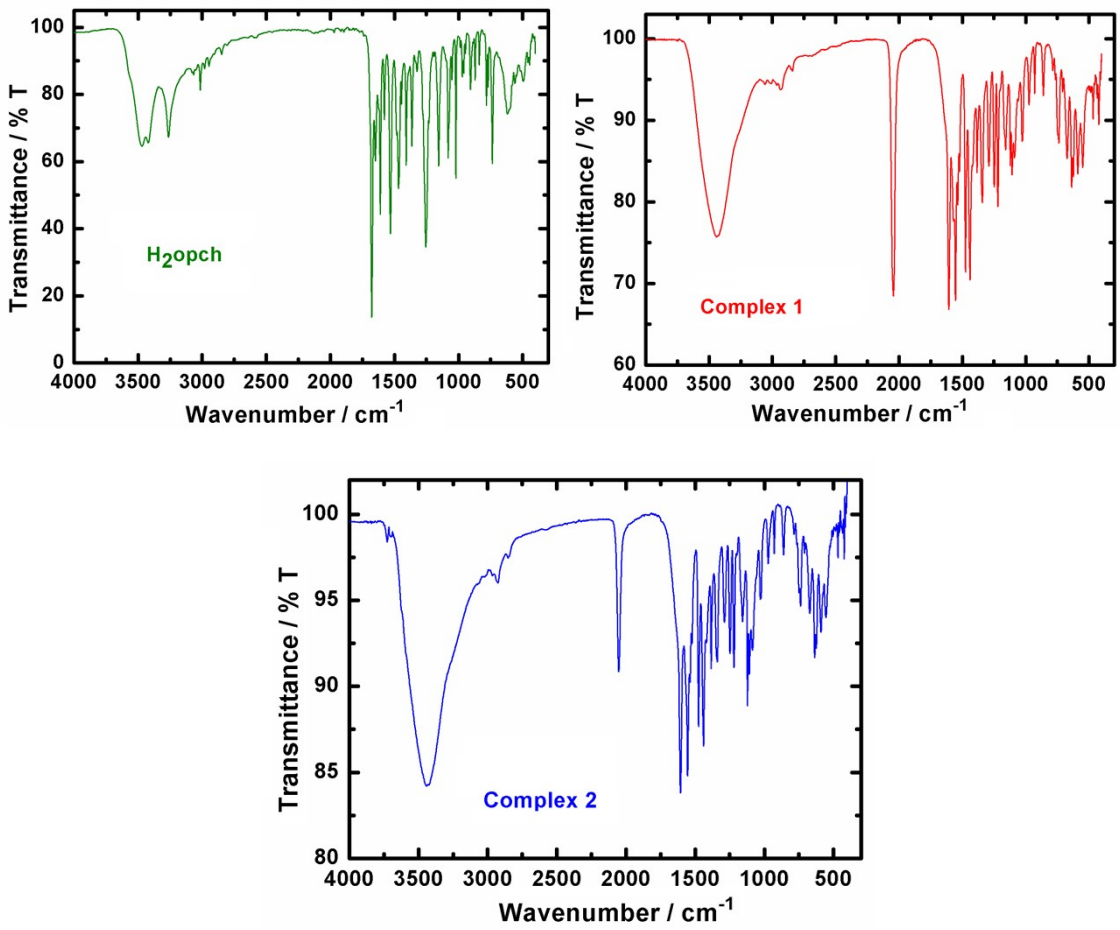

Figure S1. Infrared spectra of **H_2opch**, **1** and **2**.

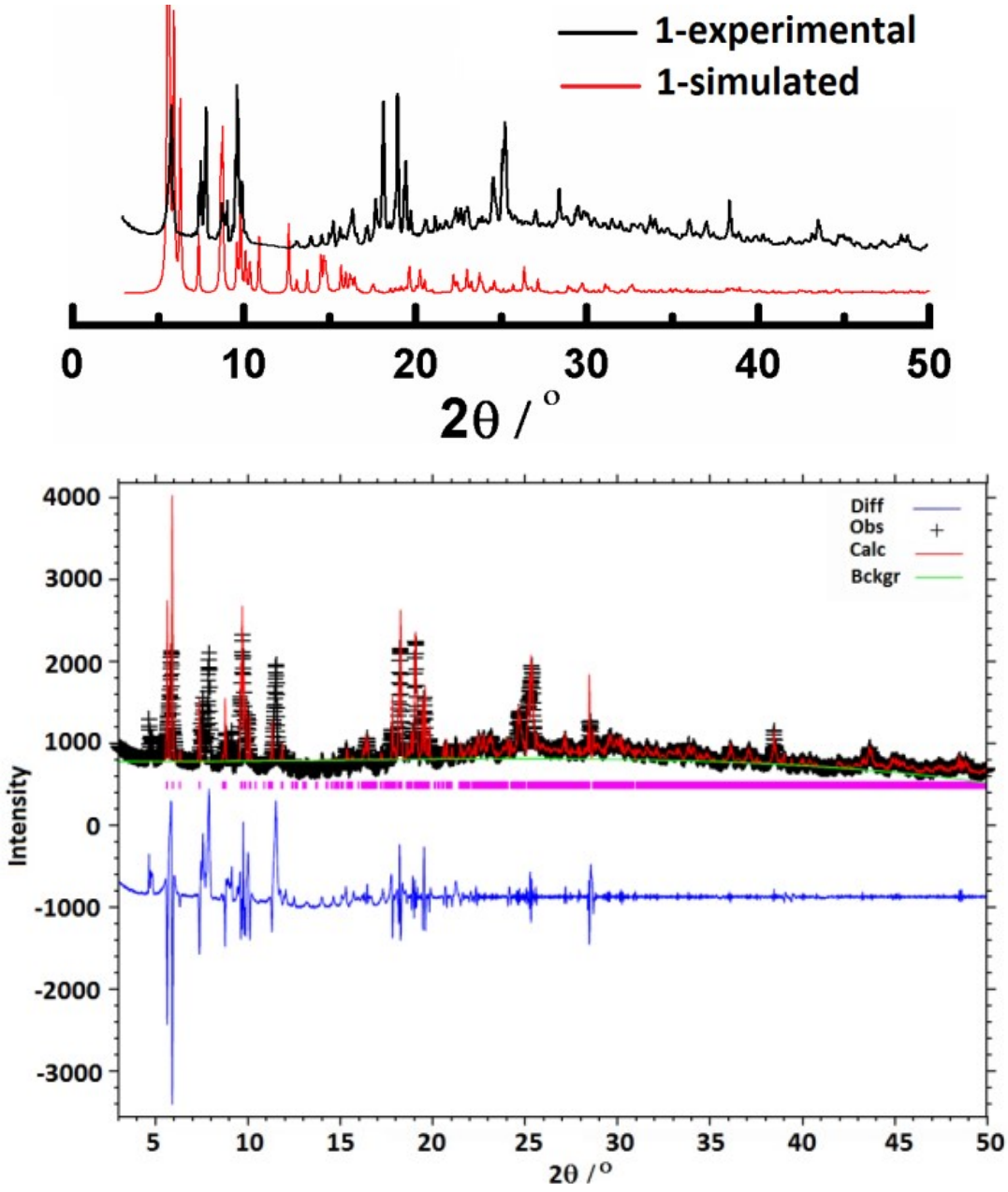

Figure S2. Top: the powder XRD patterns for complex **1**. Bottom: the black circles are for the observed data. The red solid line is for the calculated data. The grey solid curve is for the difference. The vertical bars are the positions of Bragg peaks. Cell parameters: *P*-1, a = 12.16 Å, b = 16.39 Å, c = 17.19 Å, α = 112.9°, β = 94.6°, γ = 95.8°, V = 3036.2 Å^3 (wRp = 0.145).

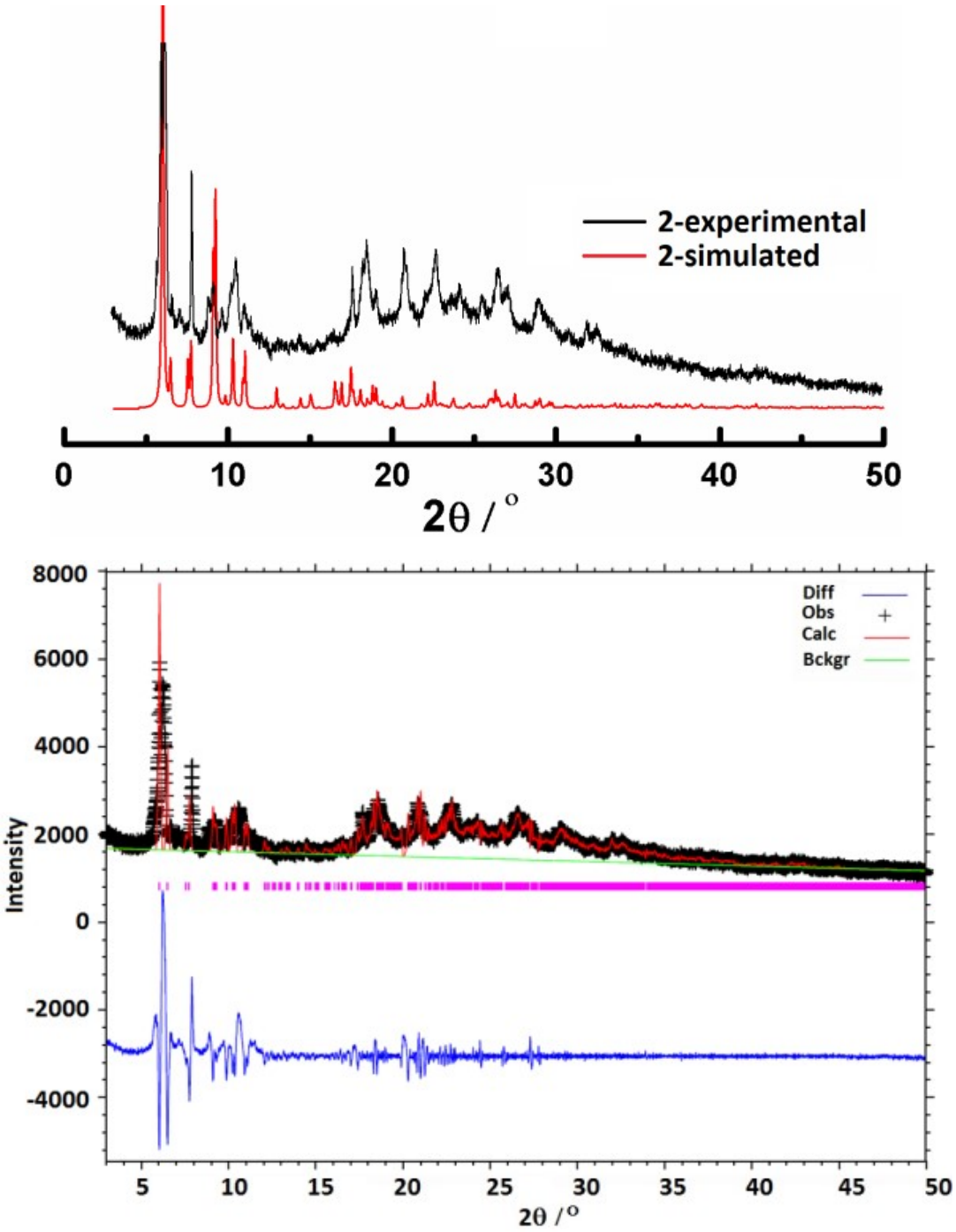

Figure S3. Top: the powder XRD patterns for complex **2**. Bottom: the black circles are for the observed data. The red solid line is for the calculated data. The grey solid curve is for the difference. The vertical bars are the positions of Bragg peaks. Cell parameters: $P2_1/c$, a = 15.54 Å, b = 19.41 Å, c = 20.21 Å, α = 90.0°, β = 109.5°, γ = 90.0°, V = 5747.4 Å^3 (wRp = 0.093).

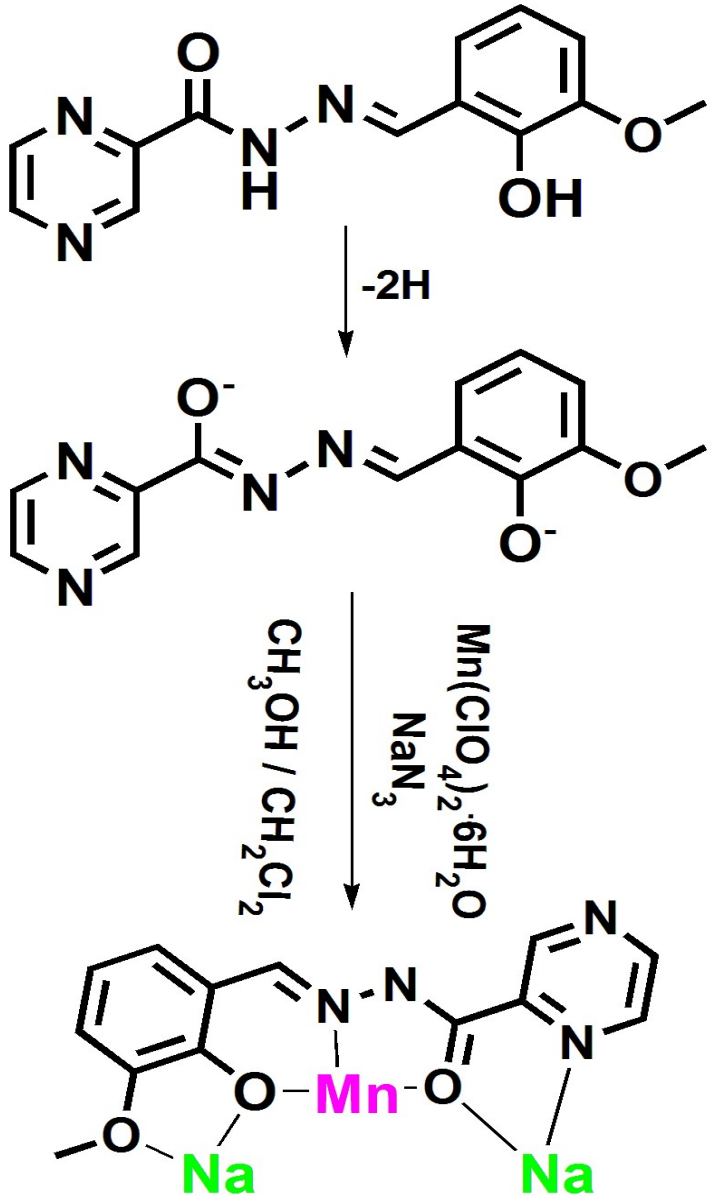

Scheme S1. H_2opch, di-deprotonated opch^{2-} and corresponding coordination mode in **1** and **2**.

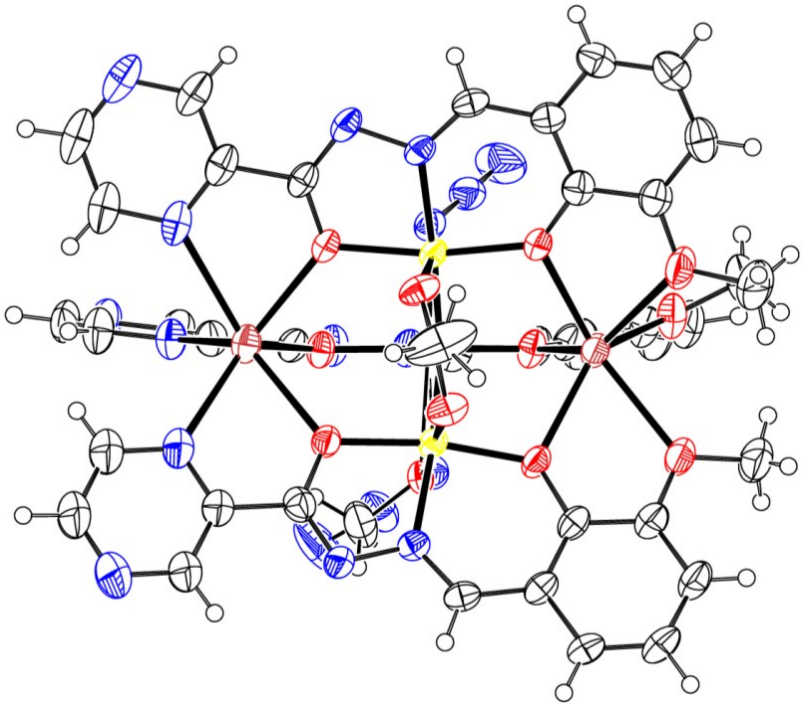

Figure S4. Structural figure of complex **1** with probability ellipsoids (probability 50%).

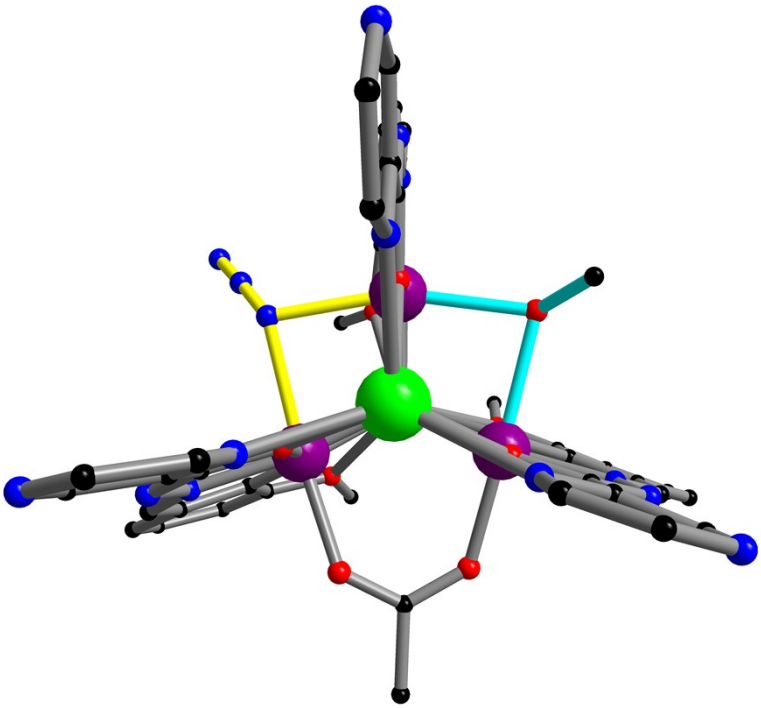

Figure S5. Top view of complex **1** in which one azide and one one methanol molecules are depicted as yellow and turquiose frames. Color scheme: violet Mn, bright green Na, red O, blue N, black C.

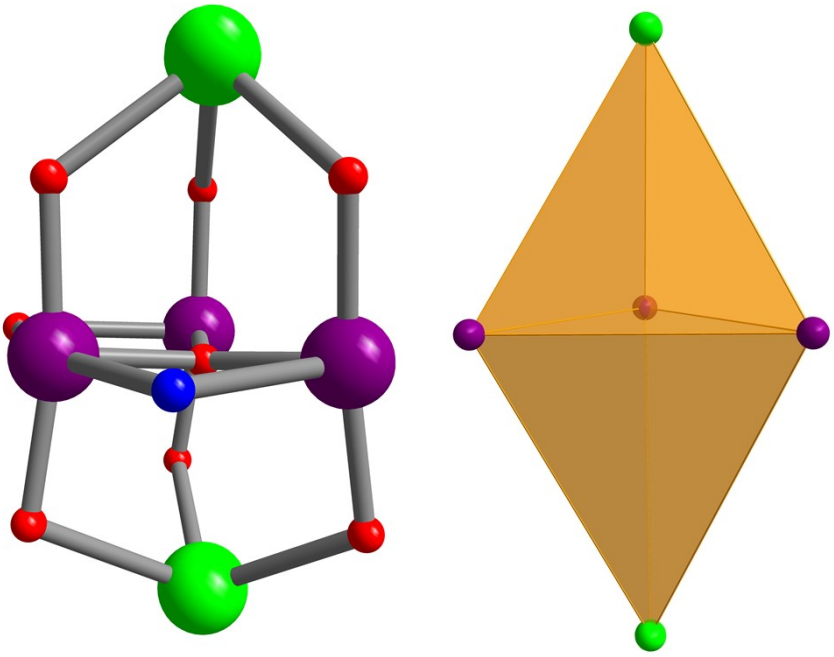

Figure S6. Left: $[Na_2Mn_3(\mu_3\text{-}O)(\mu_2\text{-}N_3)(\mu_2\text{-}O)_7]^{2+}$ core for **1**. Right: the polyhedron of Na_2Mn_3. Color scheme: violet Mn, bright green Na, red O, blue N.

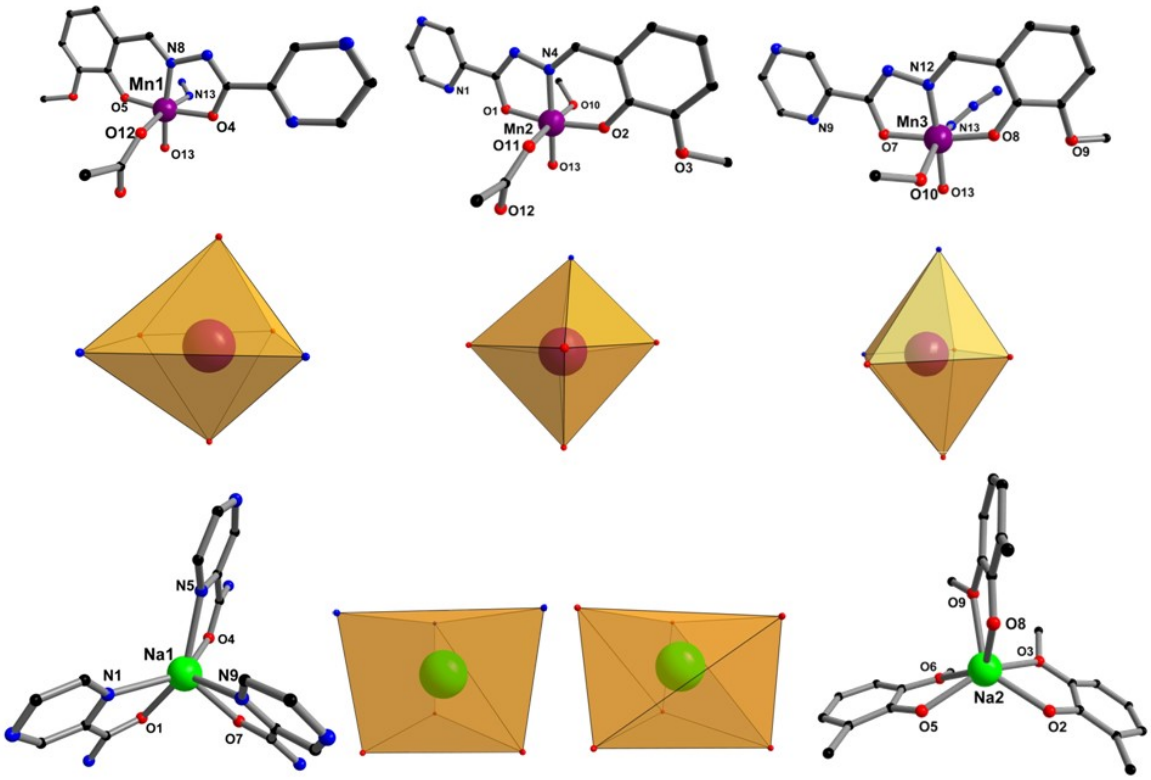

Figure S7. Coordination environments of three crystallographically independent Mn ions and two Na ions in **1**. The $spch^{2-}$ fragments are shown in gray, Mn in violet, Na in bright green, O in red, N in blue, C in black.

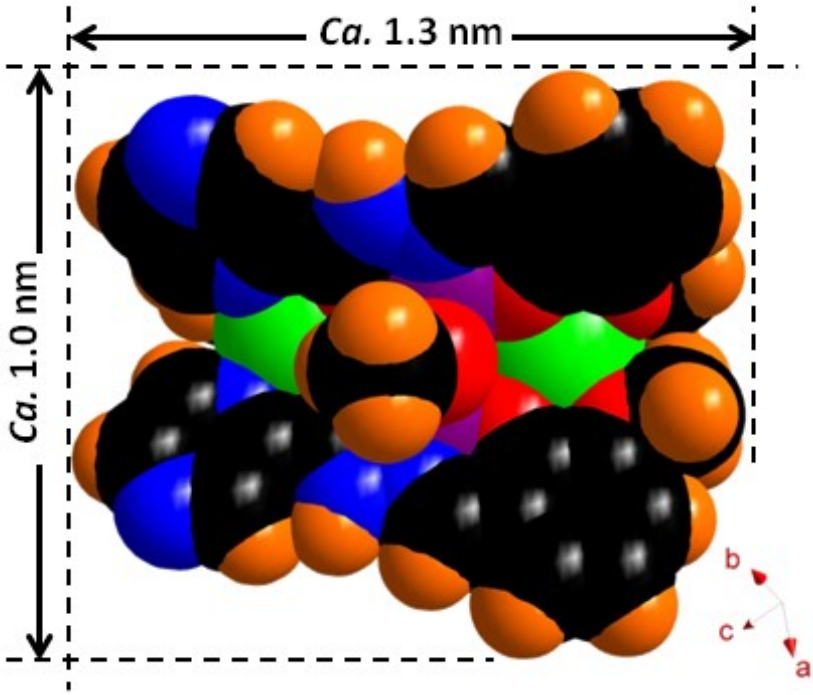

Figure S8. Space-filling representation exhibiting the longest (top) and shortest (bottom) diameters of **1**. Color code: Mn in violet, Na in bright green, O in red, N in blue, C in black, H in orange.

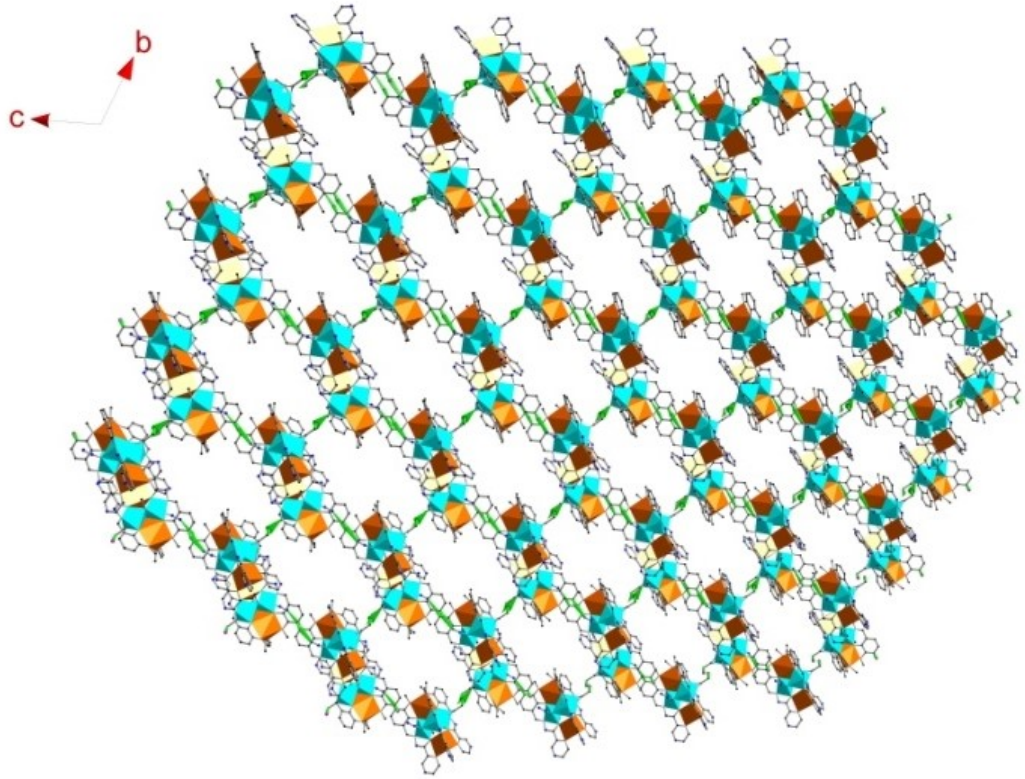

Figure S9. Illustration showing the hydrogen-bonding interactions (bright green lines) and the two-dimensional supramolecular arrangement of the molecules in **1**.

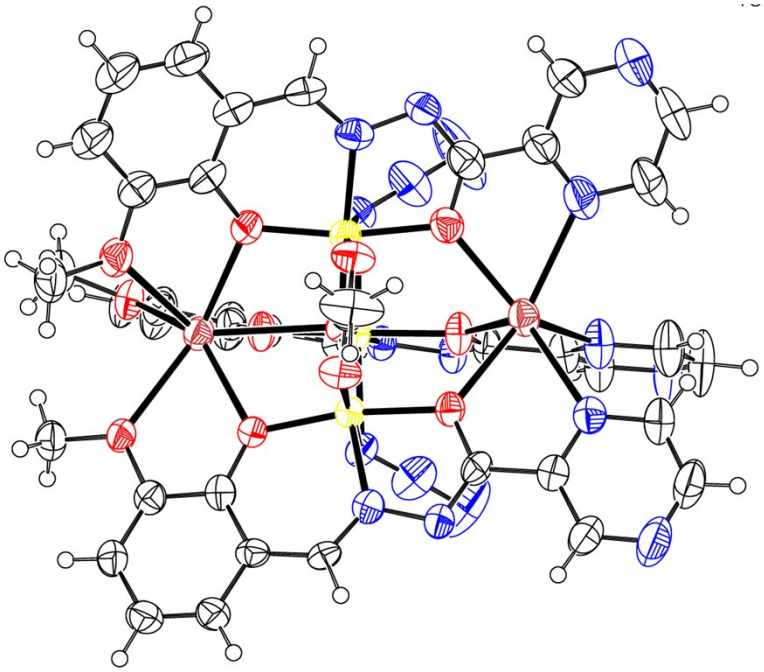

Figure S10. Structural figure of complex **2** with probability ellipsoids (probability 50%).

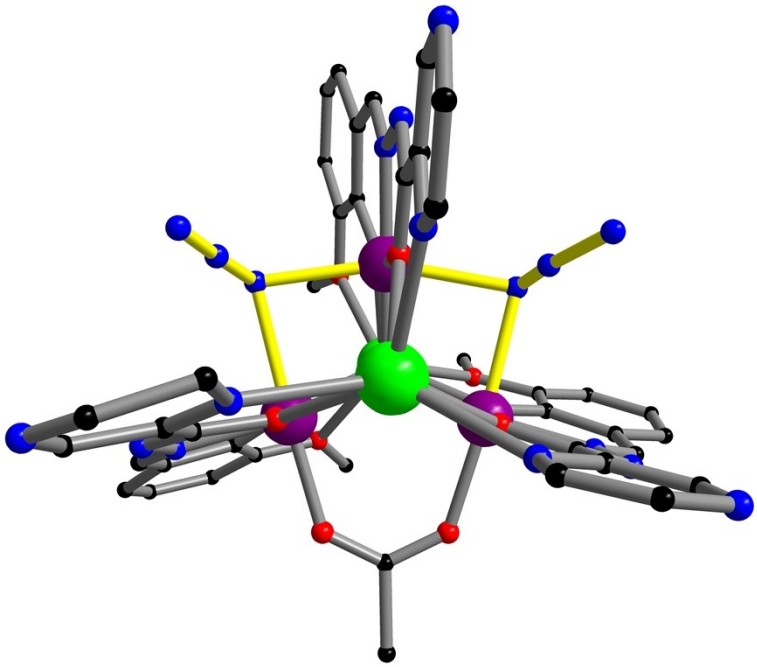

Figure S11. Top view of complex **2** in which two azide molecules are depicted as yellow frames. Color scheme: violet Mn, bright green Na, red O, blue N, black C.

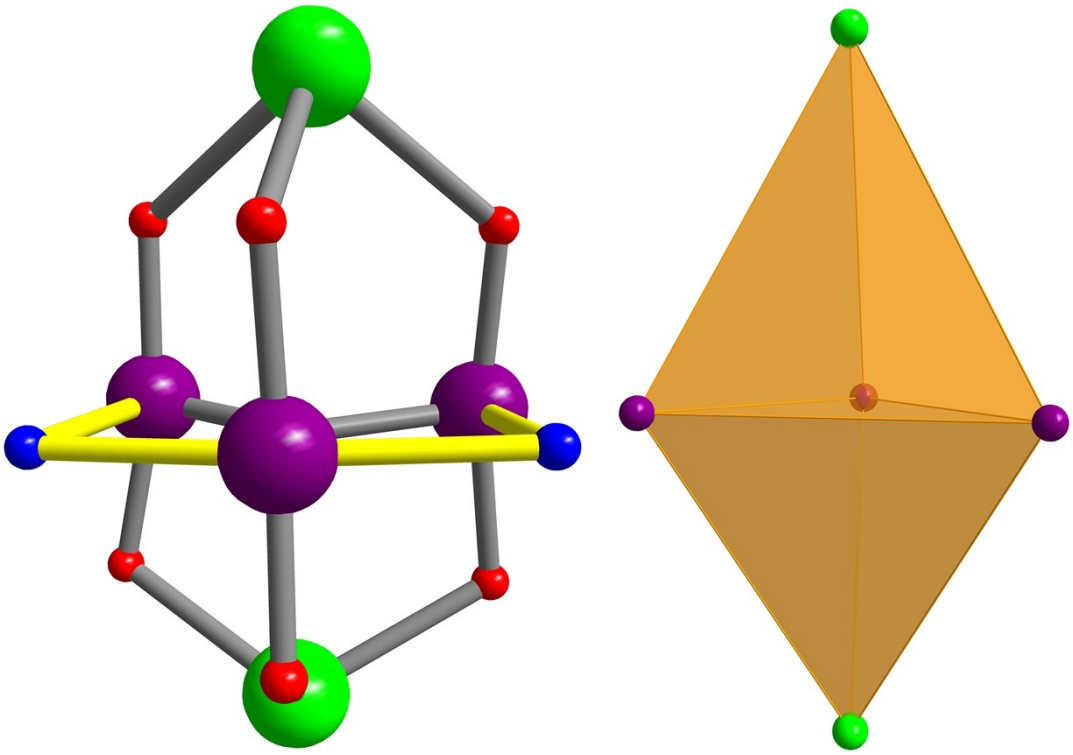

Figure S12. Left: $[Na_2Mn_3(\mu_3\text{-}O)(\mu_2\text{-}N_3)_2(\mu_2\text{-}O)_6]^{2+}$ core for **2**. Right: the polyhedron of Na_2Mn_3. Color scheme: violet Mn, bright green Na, red O, blue N.

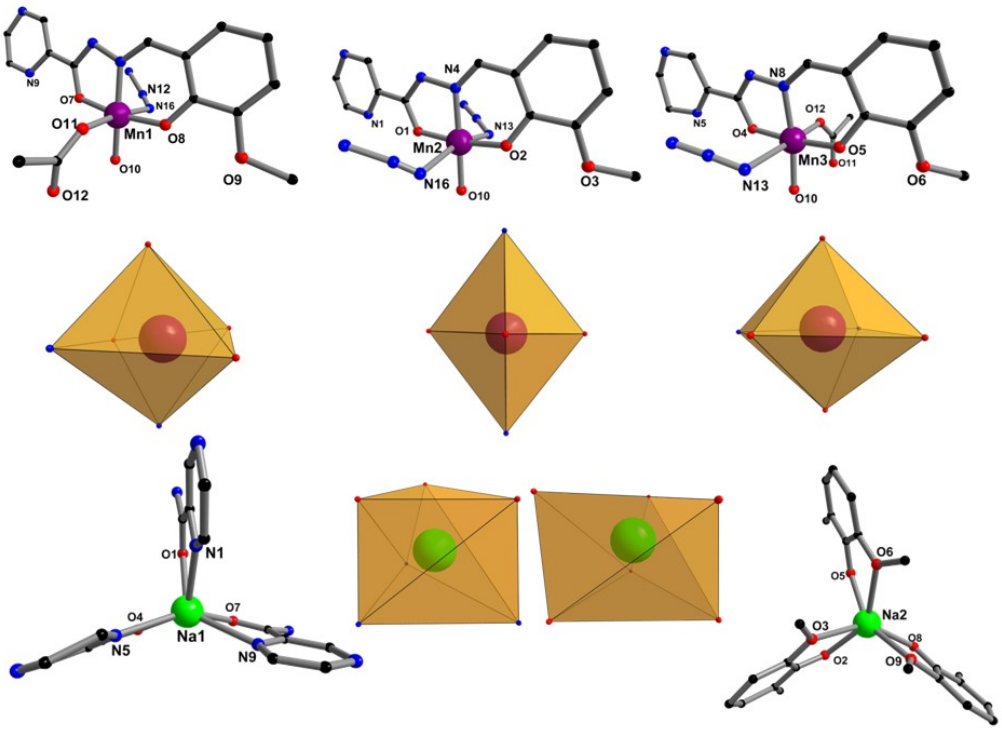

Figure S13. Coordination environments of three crystallographically independent Mn ions and two Na ions in **1**. The $spch^{2-}$ fragments are shown in gray, Mn in violet, Na in bright green, O in red, N in blue, C in black.

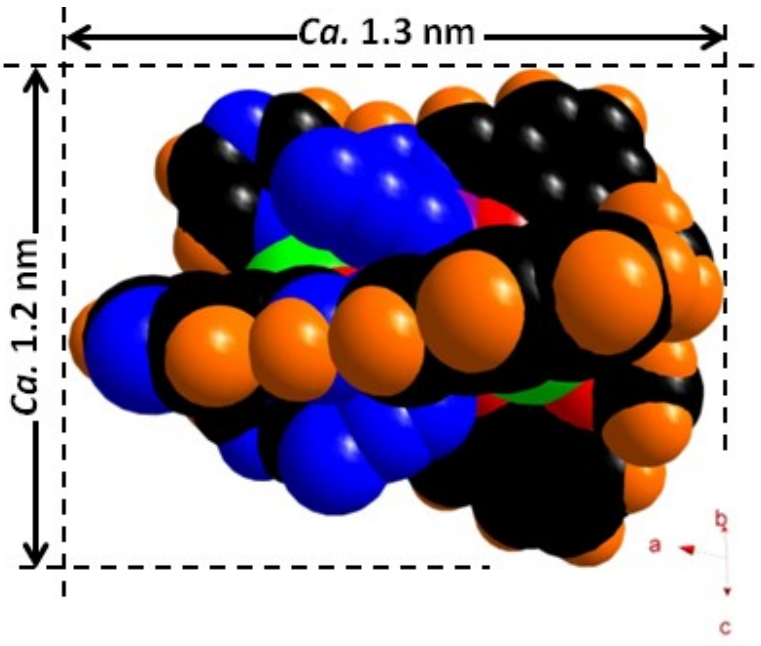

Figure S14. Space-filling representation exhibiting outer diameter (top) and thickness (bottom) of **2**. Color code: Dy in gold, O in red, P in pink, H in orange.

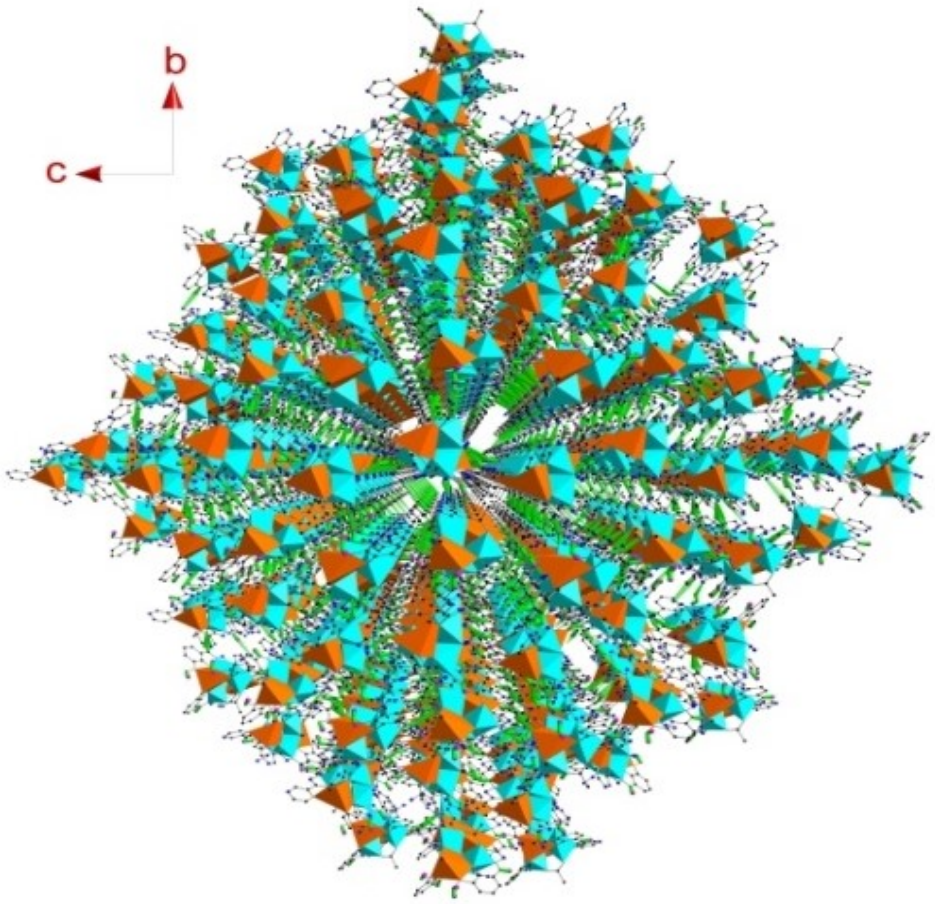

Figure S15. Illustration showing the hydrogen-bonding interactions (bright green lines) and the three-dimensional supramolecular arrangement of the molecules in **2**.

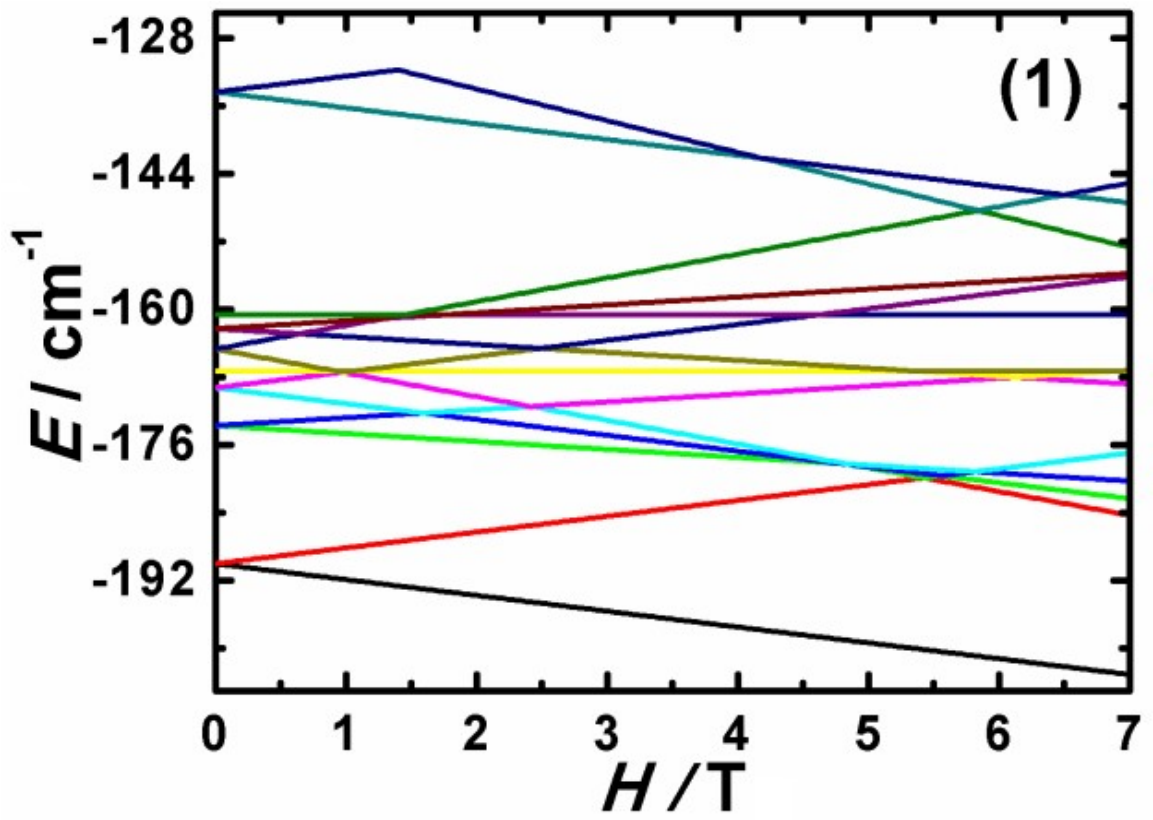

Figure S16. The fitted Zeeman splitting plot of complex **1**.

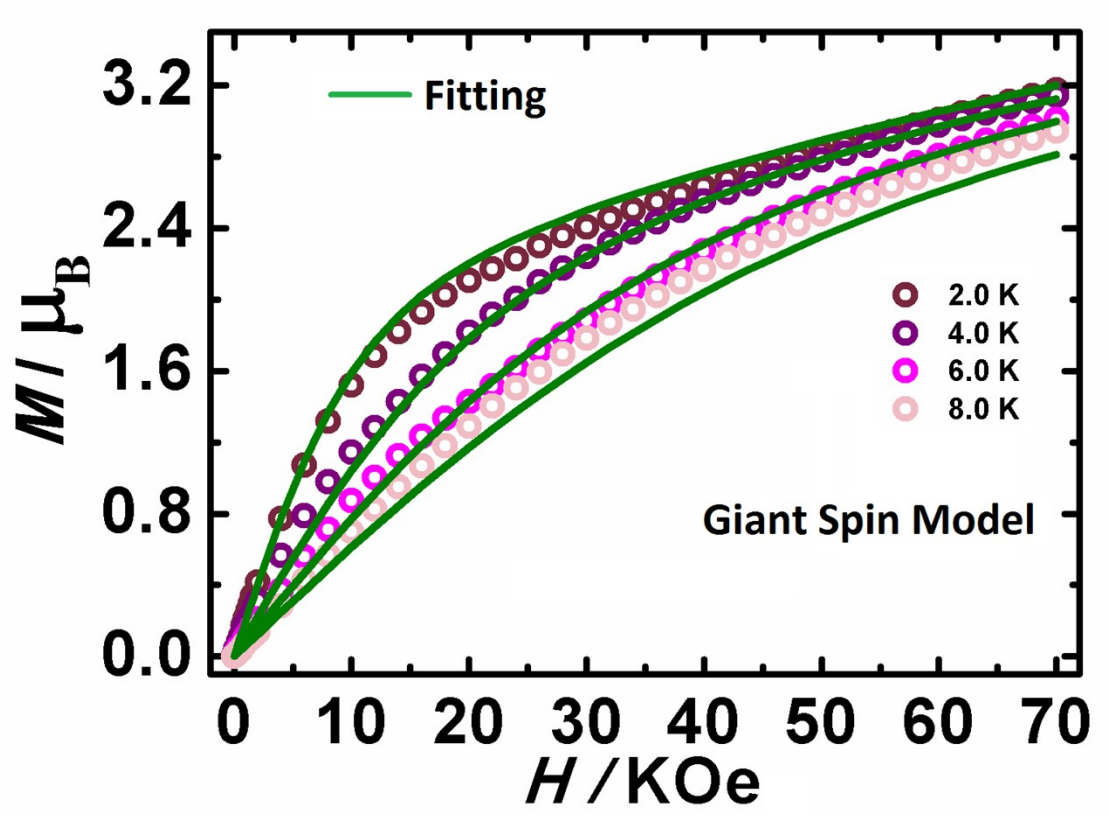

Figure S17. The *M vs. H/T* plot at different temperatures below 8.0 K for **1**. The solid line are best-fit curves with $S_T = 2$ by giant spin approximation (GSA).

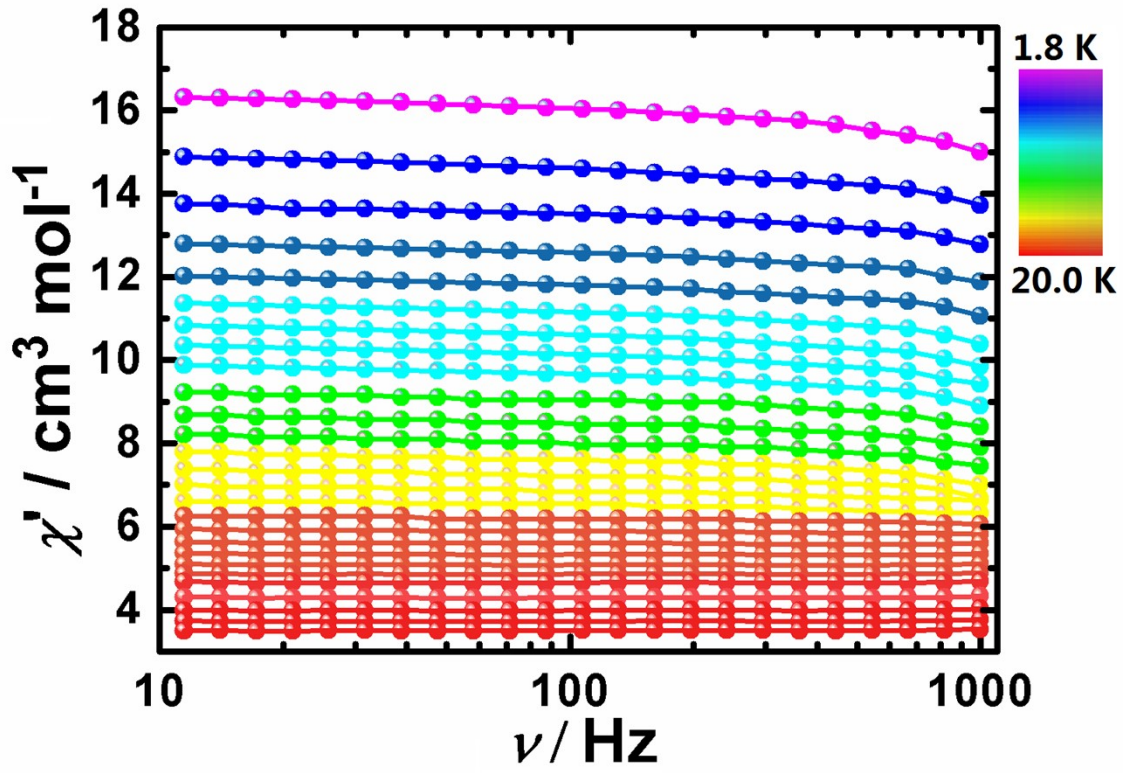

Figure S18. Frequency dependence of the χ' product, *ac* susceptibilities under zero *dc* field for **1**.

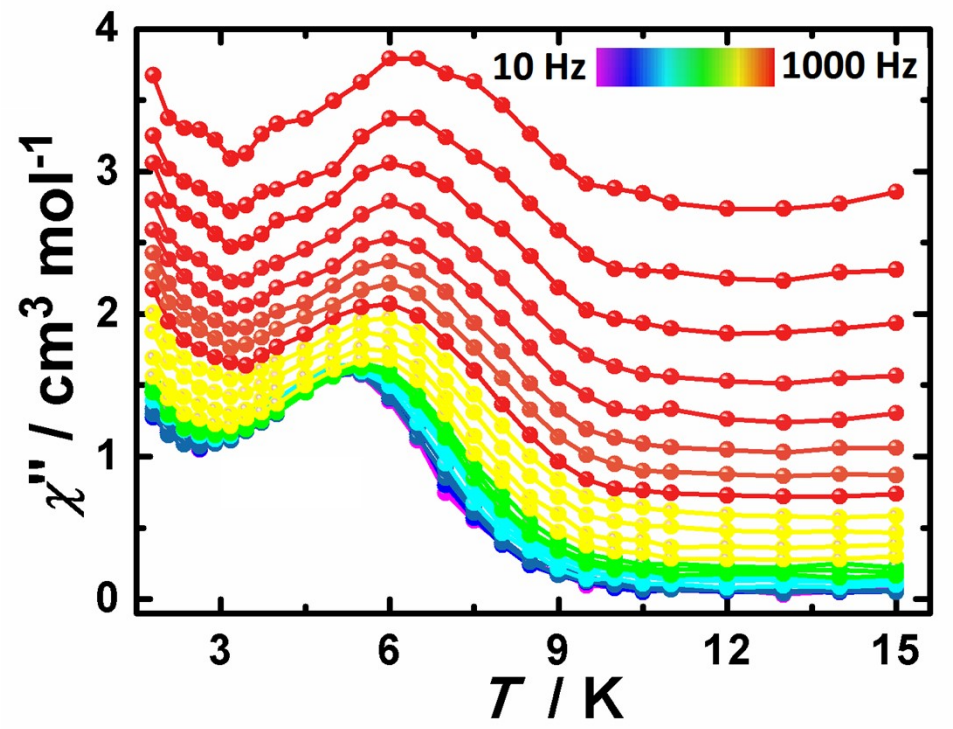

Figure S19. Temperature dependence of the χ'' product, *ac* susceptibilities under zero *dc* field for **1**.

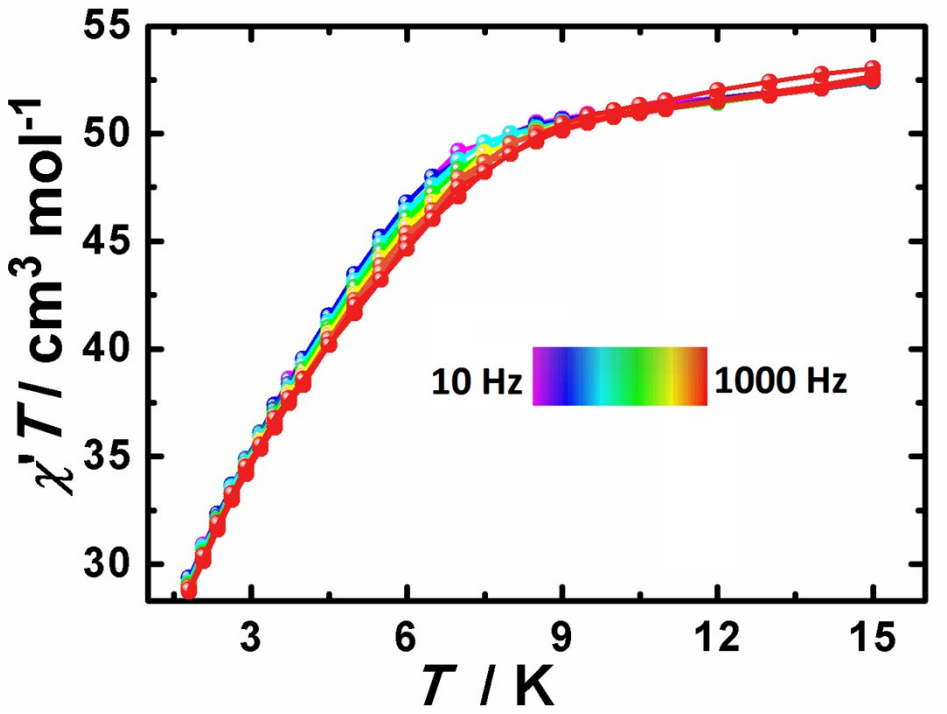

Figure S20. Temperature dependence of the $\chi'T$ product, *ac* susceptibilities under zero *dc* field for **1**.

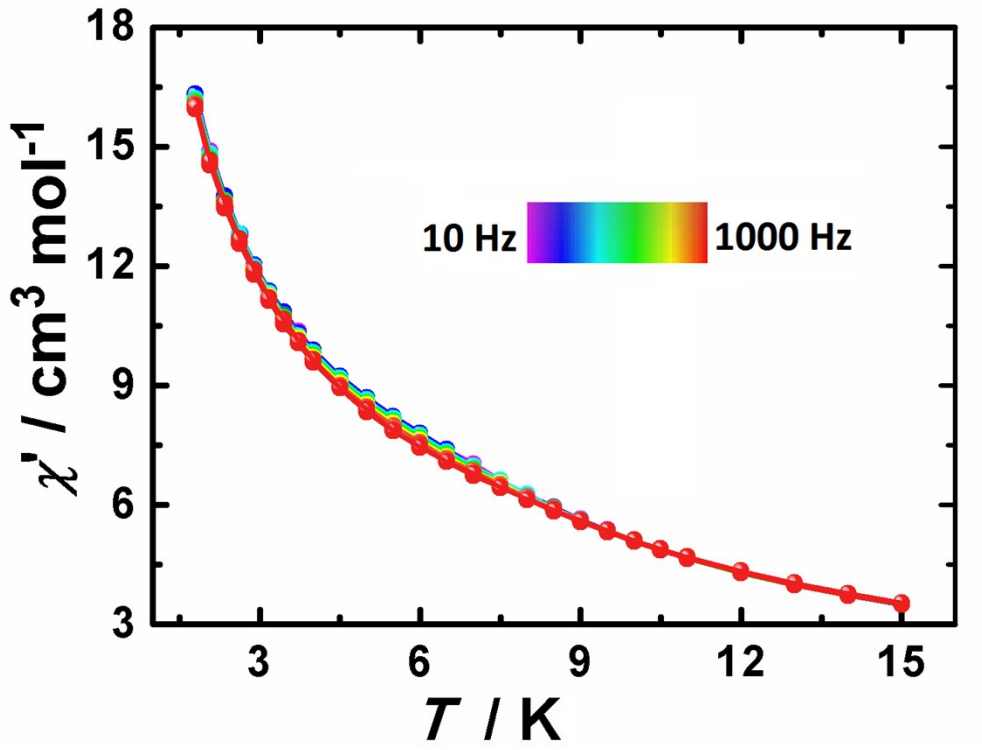

Figure S21. Temperature dependence of the χ' product, *ac* susceptibilities under zero *dc* field for **1**.

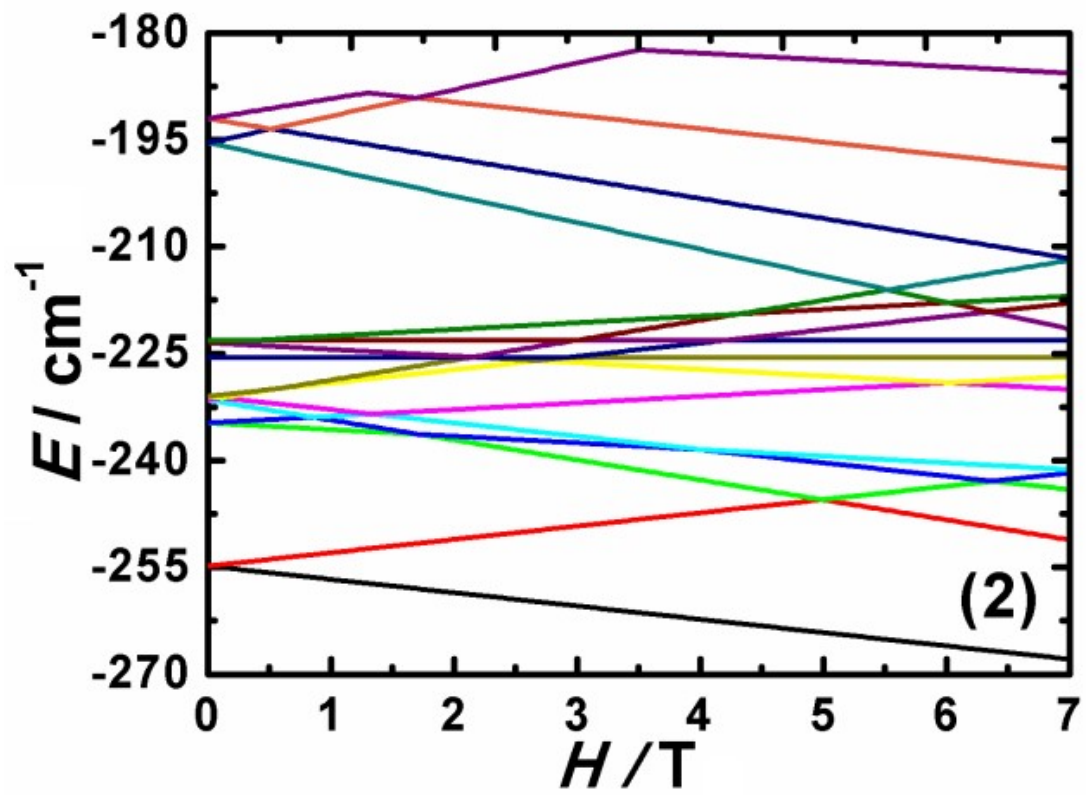

Figure S22. The fitted Zeeman splitting plot of complex **2**.

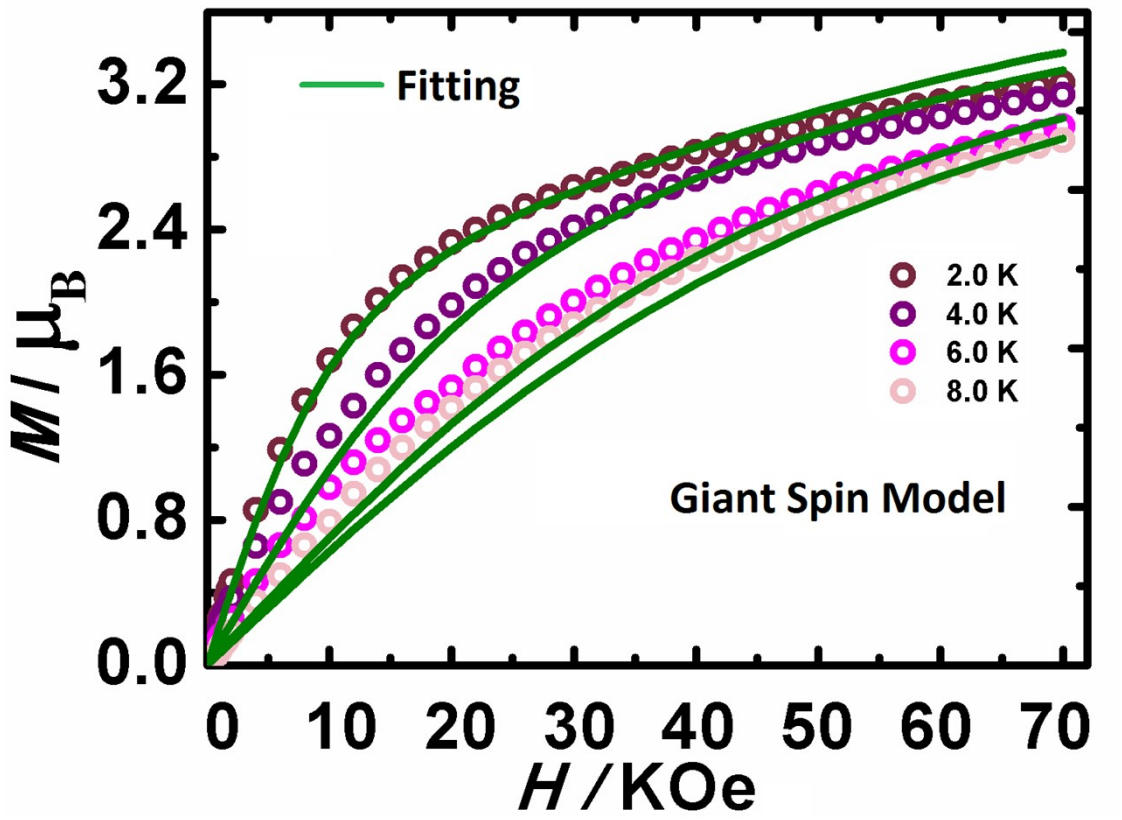

Figure S23. The *M vs. H/T* plot at different temperatures below 8.0 K for **2**. The solid line are best-fit curves with $S_T = 2$ by giant spin approximation (GSA).

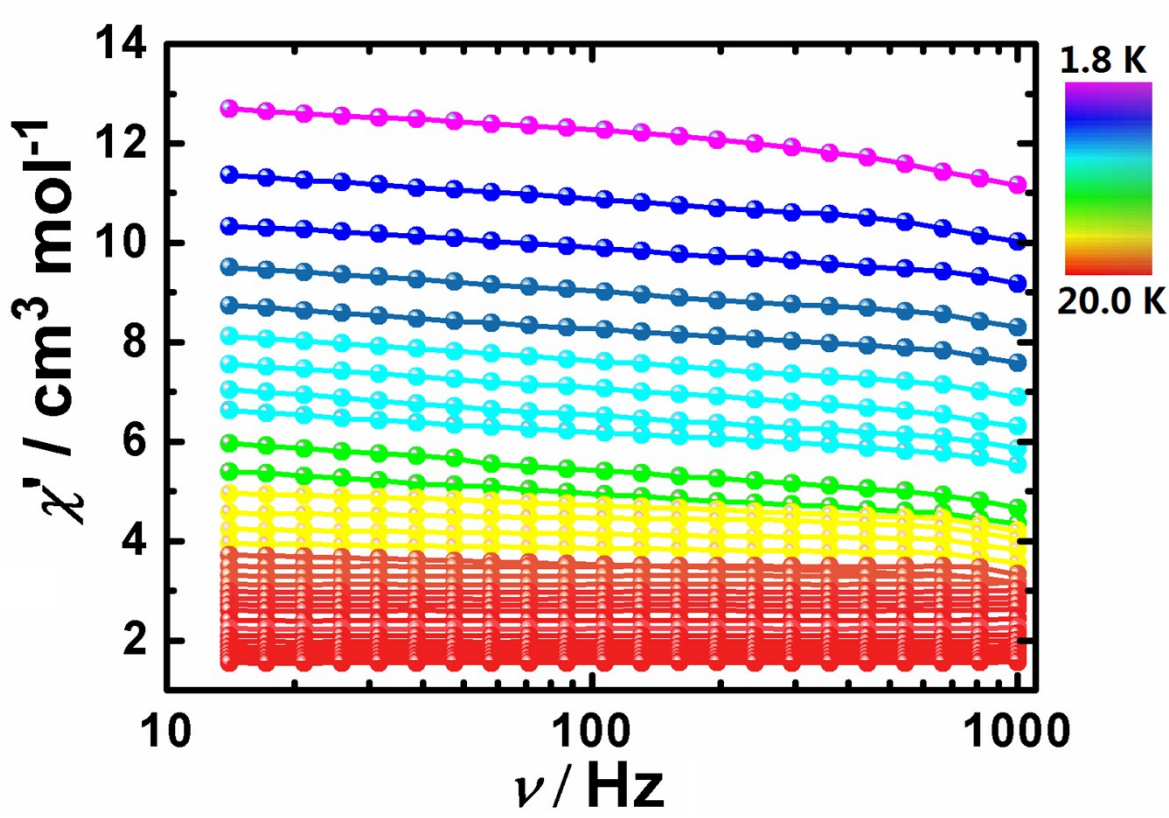

Figure S24. Frequency dependence of the χ' product, *ac* susceptibilities under zero *dc* field for **2**.

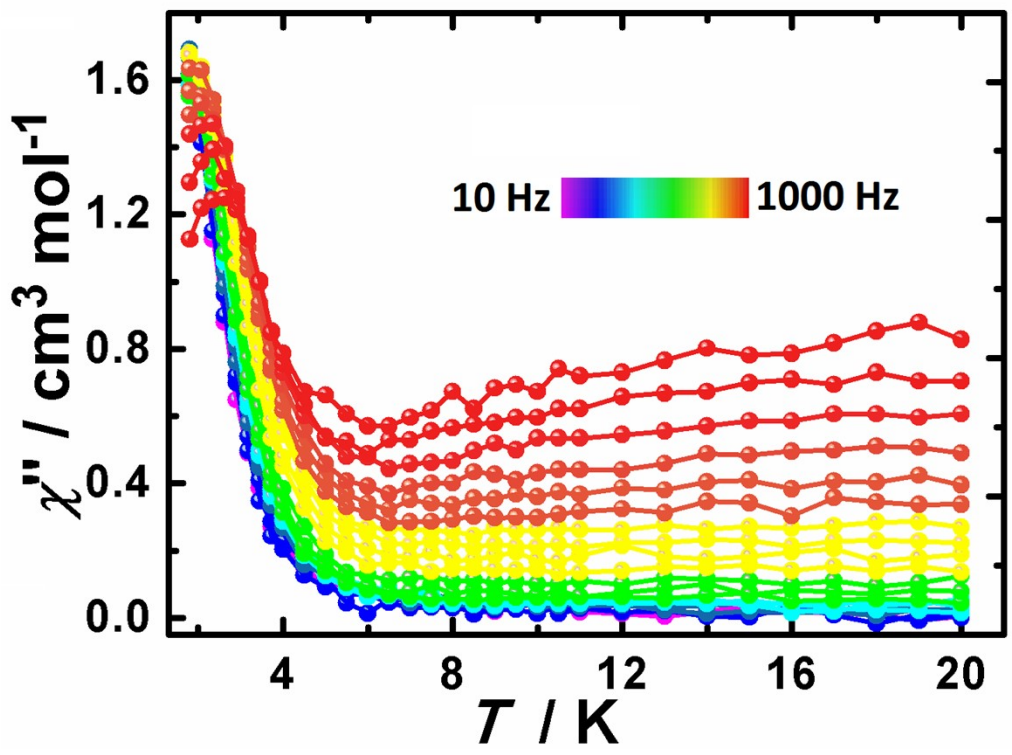

Figure S25. Temperature dependence of the χ'' product, *ac* susceptibilities under zero *dc* field for **2**.

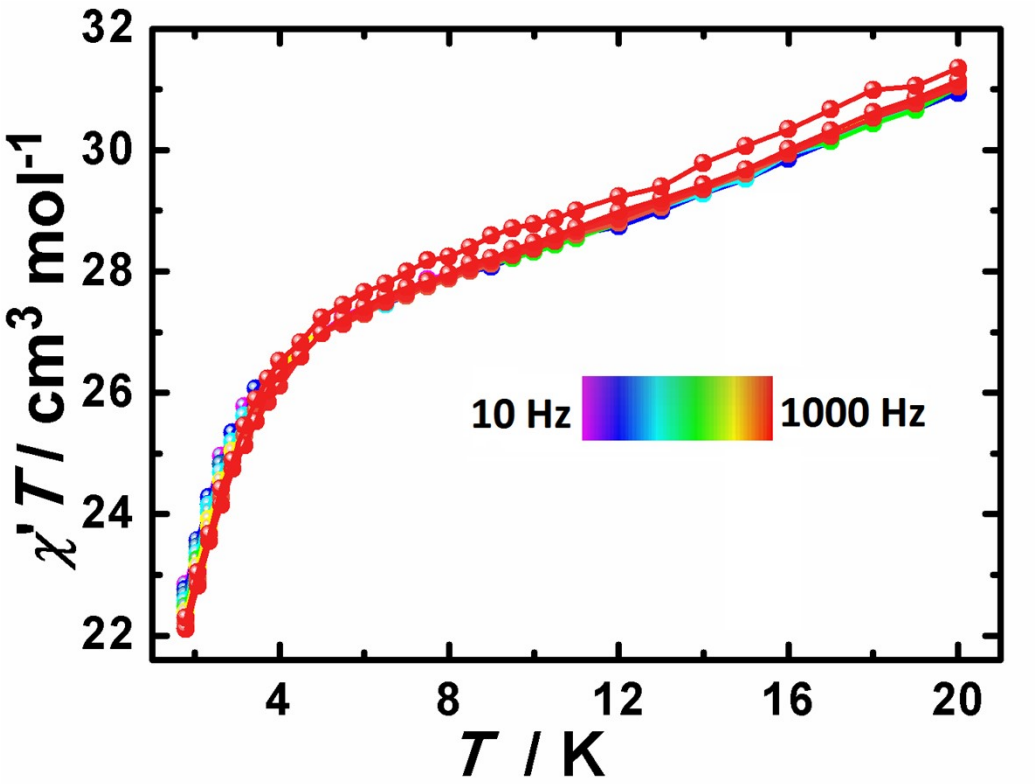

Figure S26. Temperature dependence of the $\chi'T$ product, *ac* susceptibilities under zero *dc* field for **2**.

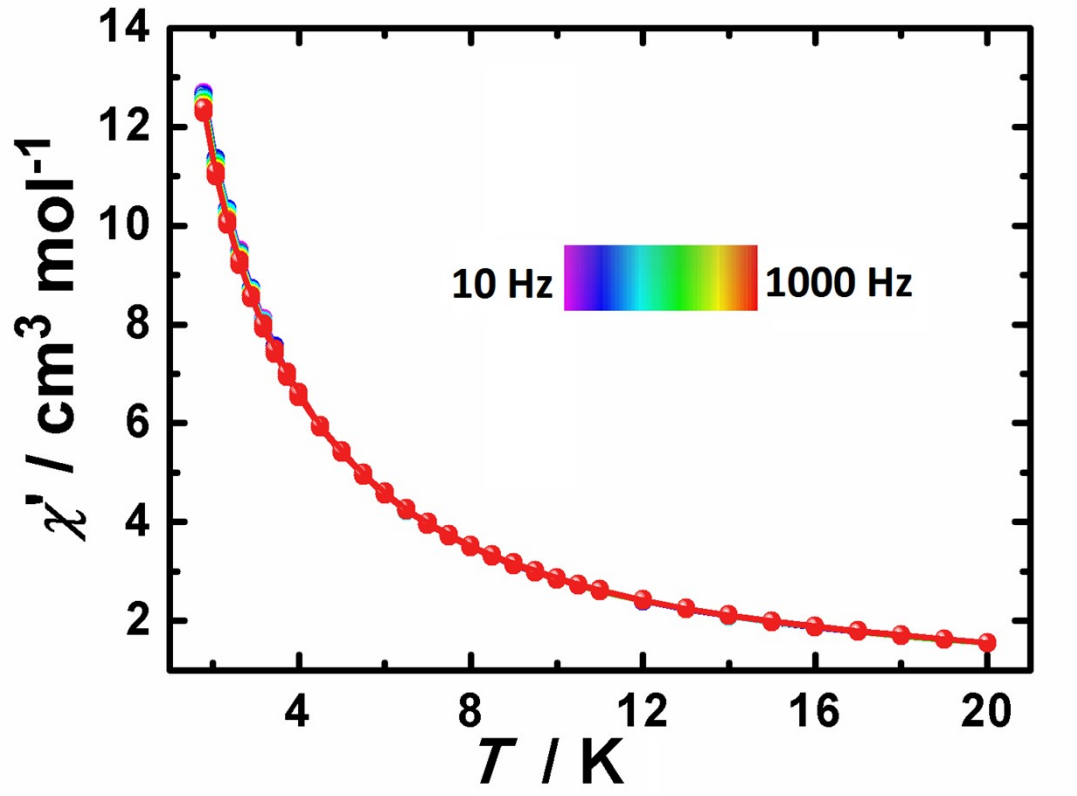

Figure S27. Temperature dependence of the χ' product, *ac* susceptibilities under zero *dc* field for **2**.

Theoretical calculation

Using the general algorithm for calculation of Heisenberg exchange constants J in multispin systems,[S1] we derived the formulas for a three-center system. Calculations of the exchange constants for three centers within BS-DFT were done by ORCA 4.2.1, UKS B3LYP functionals and DKH-def2-SVP basis set were used during calculations.

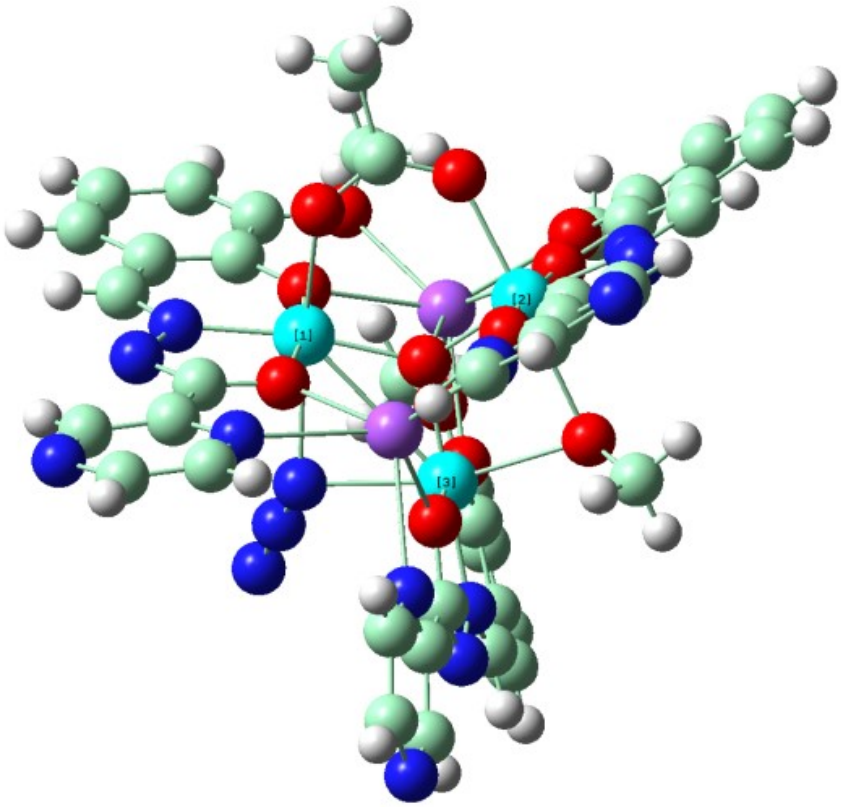

Figure S28. The calculation model of complex **1**.

Table S7. Results of BS-DFT calculations of complex **1**. Coupling constants J have been calculated with Yamaguchi's approach.

Complex 1			
State	***E* / a.u.**	**$\langle S^2 \rangle$**	***J* / cm^{-1}**
HS	-7188.605105	42.1024	
BS1	-7188.605463	10.0696	J_{12} = -11.44
BS2	-7188.605386	10.0674	J_{13} = 7.58
BS3	-7188.604078	10.0767	J_{23} = 6.53

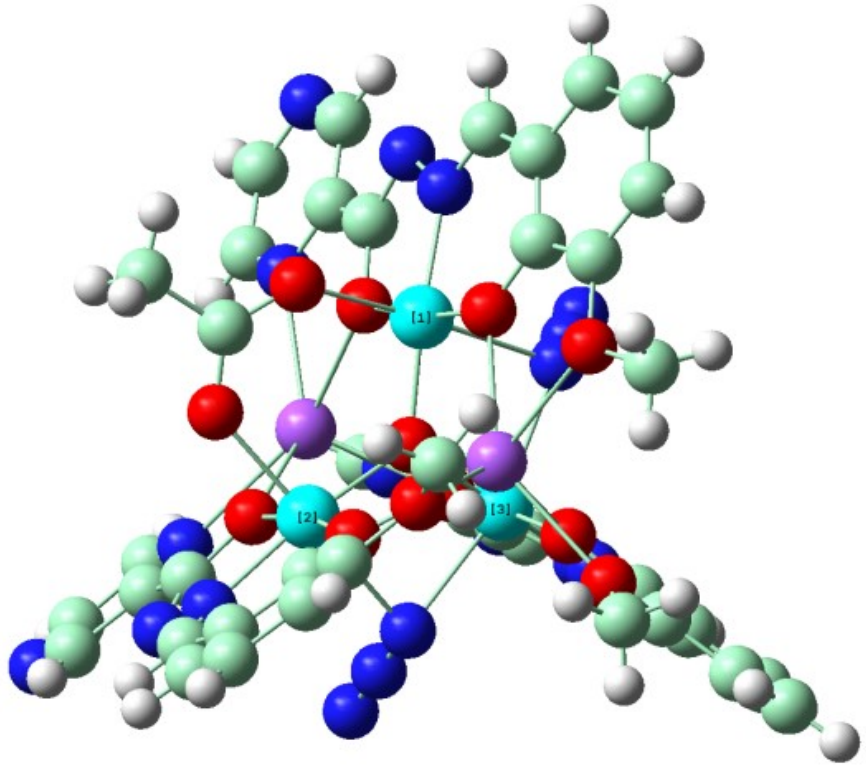

Figure S29. The calculation model of complex **2**.

Table S8. Results of BS-DFT calculations of complex **2**. Coupling constants *J* have been calculated with Yamaguchi's approach.

Complex 2			
State	***E* / a.u.**	**$\langle S^2 \rangle$**	***J* / cm^{-1}**
HS	-7237.689179	42.1113	
BS1	-7237.689399	10.0784	J_{12} = -9.77
BS2	-7237.689356	10.0792	J_{13} = 7.34
BS3	-7237.688153	10.0869	J_{23} = 6.75

References:

S1 M. Shoji, K. Koizumi, Y. Kitagawa, T. Kawakami, S. Yamanaka, M. Okumura, K. Yamaguchi, *Chem. Phys. Lett.*, **2006**, 432, 343-347.